Optical response of Al/Ti bilayer transition edge sensors*

Zhang Qing-Ya(张青雅)[a)b)], Wang Tian-Shun(王天顺)[c)d)], Liu Jian-She(刘建设)[a)b)], Dong Wen-Hui(董文慧)[a)b)], He Gen-Fang(何根芳)[a)b)], Li Tie-Fu(李铁夫)[a)b)], Zhou Xing-Xiang(周幸祥)[c)d)†], and Chen Wei(陈 炜)[a)b)‡]

[a)] *Tsinghua National Laboratory for Information Science and Technology, Tsinghua University, Beijing* 100084, *China*
[b)] *Institute of Microelectronics, Department of Micro/Nanoelectronics, Tsinghua University, Beijing* 100084, *China*
[c)] *Department of Optics and Optical Engineering, University of Science and Technology of China, Hefei* 230026, *China*
[d)] *CAS Key Laboratory of Quantum Information, University of Science and Technology of China, Hefei* 230026, *China*

(Received 4 March 2014; revised manuscript received 24 April 2014; published online 24 September 2014)

We report the optical response characteristics of Al/Ti bilayer transition edge sensors (TESs), which are mainly comprised of Al/Ti bilayer thermometers and suspended SiN membranes for thermal isolation. The measurement was performed in a ^{3}He sorption refrigerator and the device's response to optical pulses was investigated using a pulsed laser source. Based on these measurements, we obtained the effective recovery time ($\tau_{\rm eff}$) of the devices at different biases and discussed the dependence of $\tau_{\rm eff}$ on the bias. The device with a 940 μm × 940 μm continuous suspended SiN membrane demonstrated a fast response speed with $\tau_{\rm eff} = 3.9$ μs, which indicates a high temperature sensitivity ($\alpha = T/R \cdot {\rm d}R/{\rm d}T = 326$). The results also showed that the TES exhibits good linearity under optical pulses of variable widths.

Keywords: transition edge sensors, superconducting detectors

PACS: 85.25.Oj, 74.70.–b **DOI:** 10.1088/1674-1056/23/11/118502

1. Introduction

Over the last decade, transition edge sensor (TES) based detectors have been developed for the detection of photons in a large energy range, from γ-rays, X-rays to infrared photons.[1–3] TESs are usually bilayer thin films constituted by a superconductor and a normal metal layer. The superconducting proximity effect[4] between the two layers enables the tuning of the transition temperature ($T_{\rm c}$) of the bilayer, which determines the operating temperature of the detector.

An Al/Ti bilayer is a good choice for TES detectors because the two layers can be easily deposited by sputtering or e-beam evaporation at room temperature to ensure good superconducting properties. It has been adopted as thermometers in TES bolometers for millimeter wave detection.[5–7] In principle, $T_{\rm c}$ of the Al/Ti bilayer could be tuned between 390 mK ($T_{\rm c}$ of Ti bulk) and 1.1 K ($T_{\rm c}$ of Al bulk), where the Ti layer serves as the normal metal. Thus, Al/Ti bilayer TESs could be used in our liquid helium free ^{3}He sorption refrigerator, which has a minimum temperature of about 310 mK.

We recently demonstrated the capability of fabricating good quality Al/Ti bilayers by sputtering at room temperature with high thermal sensitivity ($\alpha = T/R \cdot {\rm d}R/{\rm d}T \approx 300$, calculated from the slope of the R–T curve measured under a small fixed excitation current) and tuned $T_{\rm c}$ by varying the thickness of the Ti layer.[8] We fabricated Al/Ti bilayer TESs with $T_{\rm c}$ from around 400 mK to 600 mK, which employed a suspended SiN membrane with different geometries for thermal isolation. In our previous work, we reported the noise performance of the fabricated Al/Ti bilayer TESs.[9] The TES with four 540 μm × 30 μm supporting SiN legs as the thermal links showed a noise equivalent power (NEP) around 8.0×10^{-17} W/Hz$^{1/2}$, which is good enough for some bolometric applications in astrophysics.[9]

Besides the noise performance, the response speed and the linearity of the response are two other important aspects for TESs when they are used as bolometric detectors.[10,11] In this paper, we report the optical response characteristics of the Al/Ti bilayer TESs to near infrared optical pulses generated by a pulsed laser source. The effective recovery time ($\tau_{\rm eff}$) of the TESs at different biases under different bath temperatures is measured and its dependence on the bias and the bath temperature is discussed. The results on the response of the TESs to optical pulses of variable widths are also presented.

2. Experiment

The partial microscope views of the two detectors, TES A and TES B, reported in this paper are shown in Fig. 1. The two TESs have SiN membranes with different geometries for thermal isolation. TES A consists of a 100 μm × 200 μm Al/Ti bilayer thermometer on a 940 μm × 940 μm continuous suspended SiN membrane. Figure 2 shows the cross-sectional view of TES A. In TES B, a 50 μm × 100 μm bilayer thermometer is placed on a structured suspended SiN membrane, which is comprised of a 210 μm × 370 μm suspended SiN

*Project supported by the National Basic Research Program of China (Grant No. 2011CBA00304), Tsinghua University Initiative Scientific Research Program, China (Grant No. 20131089314), and the National Natural Science Foundation of China (Grant Nos. 60836001 and 11273023).

†Corresponding author. E-mail: xizhou@ustc.edu.cn
‡Corresponding author. E-mail: weichen@tsinghua.edu.cn

© 2014 Chinese Physical Society and IOP Publishing Ltd

platform and four supporting SiN legs. The cross-sectional view of TES B is similar to that of TES A. The difference is that the continuous suspended SiN membrane in TES B is partially etched to form a SiN platform in the center and four supporting SiN legs, which work as the thermal links between the platform and the SiN/Si substrate. The SiN leg has a dimension of 540 μm × 30 μm. Four Nb leads are used to make electrical connections between the thermometers and the bonding pads in each TES. The thicknesses of the Al layer and the Ti layer are approximately 46 nm and 60 nm, respectively. The details of the device fabrication and the noise performance of TES B have been described elsewhere.[9]

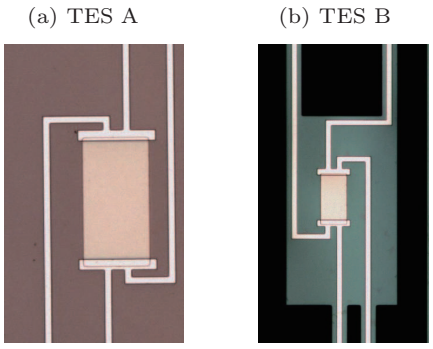


Fig. 1. (color online) Partial microscope views of two devices. (a) TES A has a 100 μm × 200 μm Al/Ti bilayer positioned on a 940 μm × 940 μm suspended SiN membrane (not fully displayed). (b) Device B has a 50 μm × 100 μm bilayer on a 210 μm × 370 μm suspended SiN platform supported by four supporting SiN legs (not fully displayed). The different color of the SiN membrane in panels (a) and (b) is due to the different light intensities of the microscope when taking these photos.

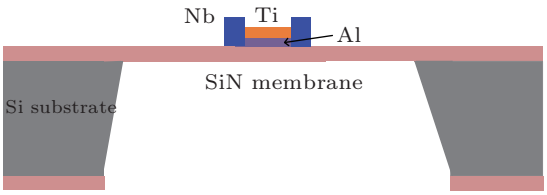


Fig. 2. (color online) The cross-sectional veiw of TES A. The Nb leads are only partially displayed and the schematic diagram is not drawn to scale for clarity.

The measurements of the TESs were performed in a liquid helium free ^{3}He sorption refrigerator. The detector chips were enclosed inside a radiation shield box made of oxygen-free high conductivity copper (OFHC), which was mounted on the mK stage of the refrigerator. The TES current versus the bias current was measured at different bath temperatures by controlling the mK stage temperature. As shown in Fig. 3, for these measurements, the voltage bias for the TES was implemented by a current (I_b) biasing a shunt resistor $R_b = 8.1$ mΩ, which was much smaller than the normal resistance (R_n) of the TES. The TES current I_{TES} was readout by a commercial superconducting quantum interference device (SQUID) amplifier, whose input inductor was connected in series to the TES. The electrical connection of the TES–SQUID branch was realized using twisted superconducting NbTi wires.

Figure 3 also shows the experimental setup for measuring the device's response to optical pulses. The optical pulses were introduced by a single mode optical fiber fed into the radiation shield box. The tip of the fiber was roughly aligned to the Al/Ti bilayer film at a distance of around 5.0 mm and the optical spot was larger than the area of the film to make sure that the device was illuminated. We used a laser source with a wavelength of 1550 nm, an optical modulator, and a variable optical attenuator to generate the optical pulses. The optical modulator was driven by a 250 Hz pulse signal generated by a function generator. The optical pulse width was determined by the width of the pulse signal, which can be varied. The SQUID output voltage pulses due to the absorption of the optical pulses were recorded by a digital oscilloscope with a bandwidth of 2 GHz.

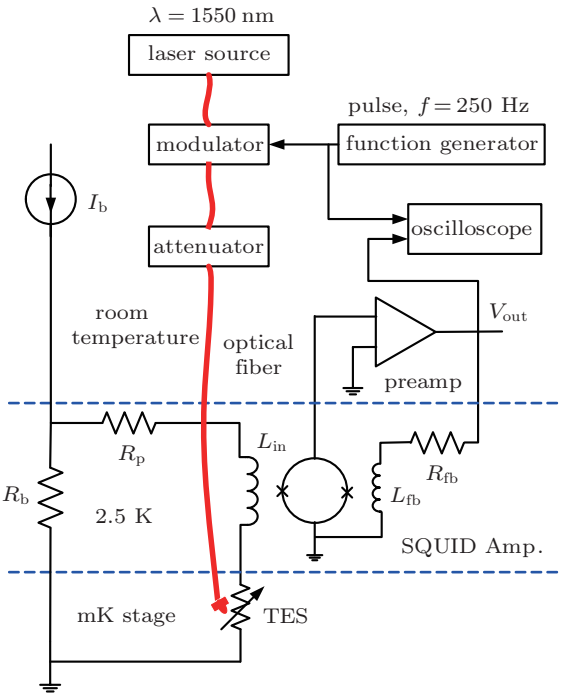


Fig. 3. (color online) Experimental setup for the TES measurement. The voltage bias for the TES is provided by a room temperature current source I_b and an 8.1 mΩ resistor R_b at 2.5 K. The TES branch has a parasitic resistance $R_p = 44$ mΩ from the wirings. The TES current is readout by a SQUID amplifier with an input inductance L_{in} of about 600 nH. The optical pulse is generated by a laser source, a modulator, and an optical attenuator.

3. Results and discussion

3.1. Device parameters

Figure 4(a) shows a typical curve of TES current I_{TES} versus bias current I_b taken from TES A at a bath temperature of 525 mK. There are three distinct regions in the curve. At a low bias current, the TES is superconducting and the curve is a straight line, as indicated by solid line 1. The parasitic resistance of the TES–SQUID branch $R_p = 44$ mΩ, which is

from the wirings, is deduced from the slope of solid line 1 and $R_b = 8.1$ mΩ. The same parasitic resistance of 44 mΩ is obtained in all experiments on both TESs. When the bias current is large ($I_b > 1.5$ mA), the TES reaches its normal state and has a constant resistance of R_n. Therefore, the I_{TES}–I_b curve becomes a straight line again, represented by solid line 2 in the figure. The slope of line 2 is set by R_n, R_p, and R_b. With known R_p and R_b, R_n can be obtained by measuring the slope of solid line 2. The intermediate region is the transition region, where the TES can be biased at different points by varying the bias current I_b. The curves of TES joule power P_{TES} and TES resistance R versus bias current I_b can be obtained according to the measured I_{TES}–I_b curve.

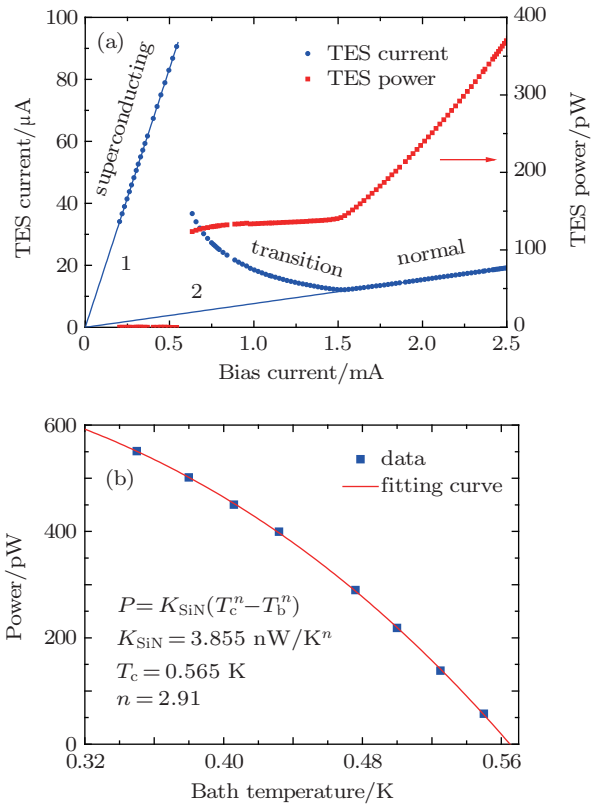


Fig. 4. (color online) (a) Measurement results of TES current versus bias current (solid circles) and TES power versus bias current (solid squares) of TES A under a bath temperature of 525 mK. (b) The data sets of power versus bath temperature and the fitting curve with Eq. (1).

In Fig. 4(a), the corresponding curve of P_{TES}–I_b is also plotted. As expected, the electrical power of the TES in the strong self-biased region is almost constant because of the negative electro-thermal feedback (ETF).[12] For the SiN membrane-isolated TES, the electrical power P of the TES in the strong self-biased region can be expressed as

$$P = K_{SiN}(T_c^n - T_b^n), \tag{1}$$

where K_{SiN} is a thermal parameter of the membrane, which could be significantly different with various membrane geometries, and n is the thermal conduction exponent. By measuring electrical power P in the self-biased region under various bath temperatures T_b and fitting the data sets of P–T_b with Eq. (1) using the least-square fit, the device parameters K_{SiN}, T_c, and n can be obtained. Figure 4(b) demonstrates the measured data sets, the fitting curve, and the obtained parameters for TES A. Then the thermal conductance of the device can be calculated according to $G = dP/dT_c = nK_{SiN}T_c^{n-1}$. The device parameters of TESs A and B are summarized in Table 1. Note that T_c of the two TESs are not the same, with a difference about 20 mK, though the two chips are from the same wafer. This may be caused by the nonuniformity of the bilayer thicknesses or the different bilayer stress due to the different membrane geometry.

Table 1. Device parameters of TESs A and B.

Parameter	TES A	TES B
TES size/μm^2	100 × 200	50 × 100
K_{SiN}/nW·K^{-n}	3.855	0.260
T_c/K	0.565	0.542
R_n/Ω	1.005	1.276
N	2.91	3.48
G/nW·K^{-1}	3.770	0.198
C/pJ·K^{-1}	0.394	0.101
τ_0/μs	104.5	509.3
τ_{eff}/μs	3.9	86.7
α	326	84

3.2. Effective recovery time

Figure 5 shows the signal response of TES B for an optical pulse with a 40 ns width, which is averaged over $N = 512$ acquired signals to minimize the effect of noise mainly from the refrigerator system. The pulse width is short enough compared to the effective recovery time (τ_{eff}) to ensure that the TES absorbs multiple photons within each pulse as a single energy-absorption event. In this measurement, the TES was operated in the transition region with $R = 0.69R_n$, $I_b = 0.63$ mA, and $T_b = 316$ mK. The averaged SQUID output voltage pulse to the optical pulse is fitted with the double-exponential function[13]

$$V_{out} = A_1 e^{-(t-t_0)/\tau_{el}} + A_2 e^{-(t-t_0)/\tau_{eff}} + B, \tag{2}$$

where A_1, A_2, t_0, and B are constants, τ_{el} represents the electrical time constant, and τ_{eff} usually dominates the response speed of the device. Here $\tau_{el} = 5.68$ μs and $\tau_{eff} = 53.61$ μs are obtained from the fitting.

By applying the same method, the averaged output voltage pulses of TESs A and B corresponding to an optical pulse with a 40 ns width at different biases through the transition region were recorded and the fitted τ_{eff} as a function of the bias (represented by the ratio of TES resistance R at the bias to R_n) were obtained. Figure 6 shows the τ_{eff} versus the bias for TESs A and B under the bath temperatures of 516 mK and 508 mK, respectively. The plots demonstrate that the detectors

have larger $\tau_{\rm eff}$ in the top and the bottom than in the middle of the transition region. This trend is similar with that obtained from an Al/Ti/Au trilayer TES.[14] This result is caused by the varying thermal sensitivity parameter α in the transition region.

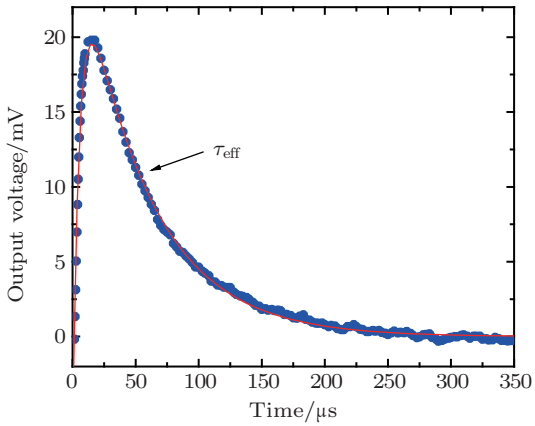


Fig. 5. (color online) The averaged output voltage pulse for a 40 ns width optical pulse (dot curve) of TES B and the fitted curve (solid line) with the double-exponential function.

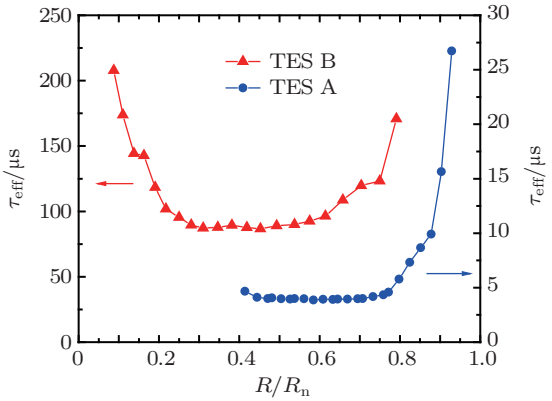


Fig. 6. (color online) The effective recovery time $\tau_{\rm eff}$ versus the bias through the transition region of TESs A and B under the bath temperatures of 516 mK and 508 mK, respectively.

When biased at $0.58R_{\rm n}$ and $0.45R_{\rm n}$, TESs A and B have minima $\tau_{\rm eff}$ of 3.9 μs and 86.7 μs, respectively. The thermal sensitivity parameter α of the Al/Ti bilayer thermometer at the bias point can be estimated according to the formula[12]

$$\tau_{\rm eff} = \frac{\tau_0}{(1+\alpha P/(GT_{\rm c}))} = \frac{C}{G\left(1+\alpha/n(1-T_{\rm b}^n/T_{\rm c}^n)\right)}, \quad (3)$$

where $\tau_0 = C/G$ is the intrinsic time constant and C is the heat capacity of the TES. Here the heat capacity of the superconducting Nb leads is neglected and the heat capacity of TES A includes the heat capacity of the bilayer and the SiN membrane underneath the film. The heat capacity of TES B includes the heat capacity of the bilayer and the central SiN platform. The specific heat of Al, Ti, and SiN are taken from the published data.[12,15] A factor of 2.43 is taken into account when calculating the heat capacity of the Al film because of the increase in heat capacity of a superconducting material at its transition temperature.[12]

Table 1 also lists the calculated C, τ_0, the minimum $\tau_{\rm eff}$, and the corresponding α estimated by Eq. (3) for the two TESs. The two TESs from the same wafer show quite different values of α, possibly because of the difference in the quality of the bilayers. The similar results were also reported in tungsten TESs from the same wafer.[16] The much faster response speed of TES A with $\tau_{\rm eff} = 3.9$ μs is due to the more sensitive bilayer thermometer with $\alpha = 326$ and the smaller $\tau_0 = 104.5$ μs owing to the larger thermal conductance. The $\tau_{\rm eff}$ as a function of the bias for TES B at the bath temperatures of 508 mK, 470 mK, and 316 mK were measured. The $\tau_{\rm eff}$ versus the bias for TES B at these three bath temperatures is shown in Fig. 7. The results overall show that the TES has a smaller $\tau_{\rm eff}$ and a faster response speed under a lower bath temperature at the same bias.

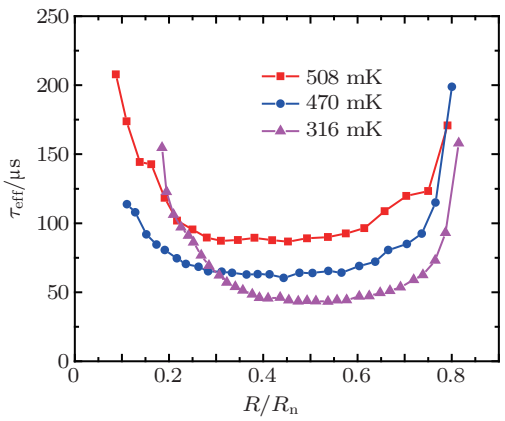


Fig. 7. (color online) The effective recovery time $\tau_{\rm eff}$ versus the bias through the transition region of TES B under three different bath temperatures of 508 mK , 470 mK, and 316 mK.

3.3. Signal response

Figure 8(a) demonstrates the averaged signal response of TES B for optical pulses with different widths ranging from 25 ns to 65 ns with the same optical source power level and fixed attenuation coefficient. In this experiment, the device was operated in the transition region with $R = 0.6R_{\rm n}$, $I_{\rm b} = 0.58$ mA, and $T_{\rm b} = 316$ mK. The $\tau_{\rm eff}$ obtained from the nine voltage pulse curves corresponding to the different absorbed energies have a mean value of 45.61 μs and a maximum absolute deviation from the mean value of no more than 1.7 μs, confirming that the device operates in the small signal limit and $\tau_{\rm eff}$ depends on the device characteristics not on the absorbed energy. Because of the strong ETF in the transition region, the energy deposited into the TES corresponds to the reduction in the electrical power supplied by the bias circuit, i.e., the integral of the current pulse times the bias voltage, holding the total power dissipated on the TES at a constant value. Therefore, the averaged absorbed energy $E_{\rm p}$ for each

pulse can be estimated by[17]

$$\begin{aligned} E_{\rm p} &= -[R_{\rm b}(I_{\rm b}-I_{\rm TES})-(R_{\rm p}I_{\rm TES})]\int_{t_0}^{t_{\rm f}} {\rm d}t\Delta I_{\rm TES}(t) \\ &\quad +(R_{\rm p}+R_{\rm b})\int_{t_0}^{t_{\rm f}} {\rm d}t\Delta I_{\rm TES}^2(t) \\ &\approx -[R_{\rm b}(I_{\rm b}-I_{\rm TES})-(R_{\rm p}I_{\rm TES})]\int_{t_0}^{t_{\rm f}} {\rm d}t\Delta I_{\rm TES}(t) \\ &= -[R_{\rm b}(I_{\rm b}-I_{\rm TES})-(R_{\rm p}I_{\rm TES})]\int_{t_0}^{t_{\rm f}} {\rm d}t(\Delta V_{\rm TES}(t)/A), \quad (4) \end{aligned}$$

where $A=-5.4\times10^6$ V/A is the gain of the SQUID amplifier. The $\Delta I_{\rm TES}^2(t)$ term in Eq. (4) is negligible because it contributes no more than 1% of the $\Delta I_{\rm TES}(t)$ term to the result in these analyses. Figure 8(b) shows the computed energy from the response curve and the amplitude of the voltage pulse versus the optical pulse width and the corresponding linear fitting curves. Here, the pulse energy is represented by $E_{\rm p}/E_\gamma$ and $E_\gamma=0.80$ eV is the single photon energy for the 1550 nm wavelength. As expected, the averaged energy of the optical pulse has a linear behavior with respect to its width. Also the amplitude of the output voltage pulse has a linear relationship with respect to the optical pulse width. Thus, the amplitude of the output voltage pulse can be considered to be proportional to the absorbed energy, the same relationship as that obtained from Ti/Au bilayer TES and Ti TES.[18,19] This result demonstrates that the device has good linearity, which is an important characteristic for the TES detectors.

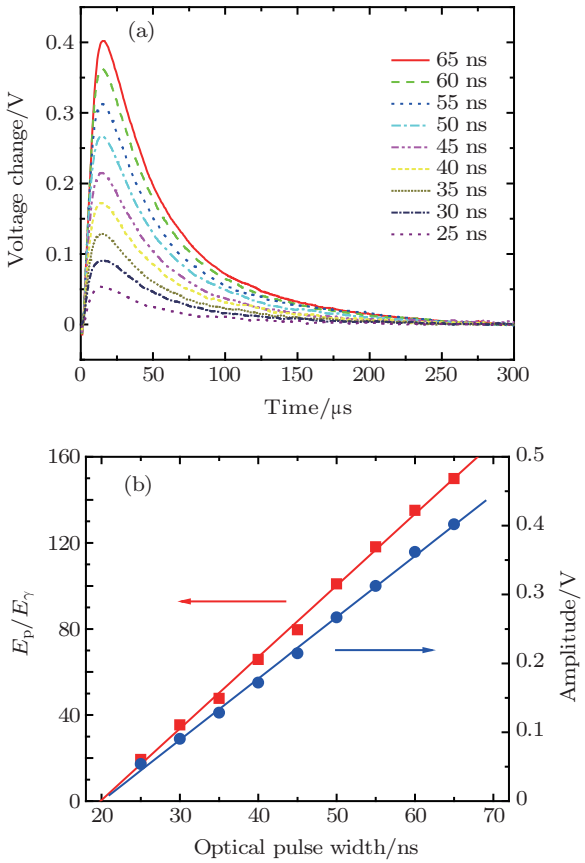


Fig. 8. (color online) TES B is operated with $R=0.6R_{\rm n}$, $I_{\rm b}=0.58$ mA, and $T_{\rm b}=316$ mK. (a) The averaged output voltage pulses for optical pulses with different widths. (b) Computed pulse energy ($E_{\rm p}/E_\gamma$) (square dots) and voltage pulse amplitude (circle dots) versus optical pulse width and the linear fitting curves (solid lines).

4. Summary

The response of Al/Ti bilayer TESs to optical pulses and the response speed of the TESs were investigated. The TESs showed good linearity to the absorbed energy and they had faster response speeds when biased in the middle part of the superconducting transition region, where the Al/Ti bilayers had a larger thermal sensitivity parameter α than that in other parts of the transition region. The results also showed that the TES had a faster response speed when working under a lower bath temperature. The TES with larger thermal conductance and higher thermal sensitivity demonstrated a fast response speed of $\tau_{\rm eff}=3.9$ μs. By integrating absorbers for specific wavelengths, Al/Ti bilayer TESs could be promising candidates for bolometric applications.

Acknowledgments

The authors would like to thank Emanuele Taralli of INRIM in Italy, Liu Cong-Zhan, Zhang Shuo, and Li Zheng-Wei of IHEP, CAS for useful discussions about the optical response measurements. Zhang Q Y would also like to thank Adrian T. Lee, Michael J. Myers, Aritoki Suzuki, and Ben Westbrook of the department of physics at UC Berkeley for their kind help on his research about TES detectors when he was a visiting student there in 2012.

References

[1] Irwin K D 1995 *Appl. Phys. Lett.* **66** 1998
[2] Doriese W B, Ullom J N, Beall J A, Duncan W D, Ferreira L, Hilton G C, Horansky R D, Irwin K D, Mates J A B, Reintsema C D, Vale L R, Xu Y and Zink B L 2007 *Appl. Phys. Lett.* **90** 193508
[3] Cabrera B, Claarke R M, Colling P, Miller A J, Nam S and Romani R W 1998 *Appl. Phys. Lett.* **73** 735
[4] Martinis J M, Hilton G C, Irwin K D and Wollman D A 2000 *Nucl. Instrum. Methods A* **444** 23
[5] Myers M J, Holzapfel W, Lee A T, O'Brient R, Richards P L and Tran H T 2005 *Appl. Phys. Lett.* **86** 114103
[6] Suzuki A, Arnold K, Edwards J, Engargiola G, Ghribi A, Holzapfel W, Lee A, Meng X, Myers M, O'Brient R, Quealy E, Rebeiz G and Richards P 2012 *J. Low Temp. Phys.* **167** 852
[7] Westbrook B, Lee A, Meng X, Suzuki A, Arnold K, Shirokoff E, George E, Aubin F, Dobbs M, Macdermid K, Hanany S, Raach K, Aboobaker A, Hubmayr J, Oshima T, Kawamura M and Kohno K 2012 *J. Low Temp. Phys.* **167** 885
[8] Zhang Q, Dong W, Wang T, Chen J, Liu J, Li T, Zhou X and Chen W 2014 *Chin. J. Low. Temp. Phys.* **36** 7
[9] Zhang Q, Liu J, Dong W, Wang T, He G, Li T, Zhou X and Chen W 2014 *Chin. Sci. Bull.* **59** 2292
[10] Brevik J A, Aikin R W, Amiri M, *et al.* 2010 *Proceeding of SPIE* 7741, *Millimeter, Submillimeter, and Far-infrared Detectors and Instrumentation for Astronomy V*, 77411H

[11] George E M, Ade P, Aird K A, *et al.* 2012 *Proceeding of SPIE* 8452, *Millimeter, Submillimeter, and Far-infrared Detectors and Instrumentation for Astronomy VI*, 84521F
[12] Irwin K D and Hilton G C 2005 *Topics Appl. Phys.* **99** 63
[13] Taralli E, Portesi C, Rocci R, Rajteri M and Monticone E 2009 *IEEE Trans. Appl. Supercon.* **19** 493
[14] Hunt C L 2004 *Transition-Edge Superconducting Antenna-Coupled Bolometer* (Ph.D. dissertation) (Pasadena: California Institute of Technology)
[15] Turner A D, Bock J J, Beeman J W, Glenn J, Hargrave P C, Hristov V V, Nguyen H T, Rahman F and Sethurman S 2001 *Appl. Opt.* **40** 4921
[16] Rosenberg D, Lita A E, Miller A J, Nam S and Schwall R E 2005 *IEEE Trans. Appl. Supercon.* **15** 575
[17] Lolli L 2012 *Photon-Number Resolving by Superconductive Devices* (Ph. D. dissertation) (Torino: Istituto Nazionale di Ricerca Metrologica)
[18] Rajteri M, Taralli E, Portesi C, Monticone E and Beyer J 2009 *Metrologia* **46** S283
[19] Fukuda D, Damayanthi R M T, Yoshizawa A, Zen N, Takahashi H, Amemiya K and Ohkubo M 2007 *IEEE Trans. Appl. Supercon.* **17** 259